

Durham Research Online

Deposited in DRO:

25 June 2019

Version of attached file:

Accepted Version

Peer-review status of attached file:

Peer-reviewed

Citation for published item:

Wang, Jun and Hu, Zhenbo and Pan, Baotian and Li, Menghao and Dong, Zijuan and Li, Xiaohua and Li, Xiaoqiang and Bridgland, David (2019) 'Spatial distribution pattern of channel steepness index as evidence for differential rock uplift along the eastern Altun Shan on the northern Tibetan Plateau.', *Global and planetary change.*, 181 . p. 102979.

Further information on publisher's website:

<https://doi.org/10.1016/j.gloplacha.2019.102979>

Publisher's copyright statement:

© 2019 This manuscript version is made available under the CC-BY-NC-ND 4.0 license
<http://creativecommons.org/licenses/by-nc-nd/4.0/>

Additional information:

Use policy

The full-text may be used and/or reproduced, and given to third parties in any format or medium, without prior permission or charge, for personal research or study, educational, or not-for-profit purposes provided that:

- a full bibliographic reference is made to the original source
- a [link](#) is made to the metadata record in DRO
- the full-text is not changed in any way

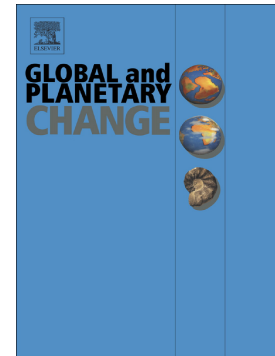
The full-text must not be sold in any format or medium without the formal permission of the copyright holders.

Please consult the [full DRO policy](#) for further details.

Accepted Manuscript

Spatial distribution pattern of channel steepness index as evidence for differential rock uplift along the eastern Altun Shan on the northern Tibetan Plateau

Jun Wang, Zhenbo Hu, Baotian Pan, Menghao Li, Zijuan Dong, Xiaohua Li, Xiaoqiang Li, David Bridgland



PII: S0921-8181(19)30029-3
DOI: <https://doi.org/10.1016/j.gloplacha.2019.102979>
Article Number: 102979
Reference: GLOBAL 102979
To appear in: *Global and Planetary Change*
Received date: 16 January 2019
Revised date: 15 June 2019
Accepted date: 15 June 2019" role="suppressed"

Please cite this article as: J. Wang, Z. Hu, B. Pan, et al., Spatial distribution pattern of channel steepness index as evidence for differential rock uplift along the eastern Altun Shan on the northern Tibetan Plateau, *Global and Planetary Change*, <https://doi.org/10.1016/j.gloplacha.2019.102979>

This is a PDF file of an unedited manuscript that has been accepted for publication. As a service to our customers we are providing this early version of the manuscript. The manuscript will undergo copyediting, typesetting, and review of the resulting proof before it is published in its final form. Please note that during the production process errors may be discovered which could affect the content, and all legal disclaimers that apply to the journal pertain.

Spatial distribution pattern of channel steepness index as evidence for differential rock uplift along the eastern Altun Shan on the northern Tibetan Plateau

Jun Wang^{a,b}, Zhenbo Hu^{a,*} zhbhu@lzu.edu.cn; hu_zhb@126.com, Baotian Pan^{a,*}, Menghao Li^a, Zijuan Dong^a, Xiaohua Li^a, Xiaoqiang Li^b, David Bridgland^c

^aKey Laboratory of Western China's Environmental Systems (Ministry of Education), College of Earth and Environmental Sciences, Lanzhou University, Lanzhou 730000, People's Republic of China

^bGeological Survey of Gansu Province, Lanzhou 730000, People's Republic of China

^cDepartment of Geography, Durham University, South Road, Durham, DH1 3LE, UK

*Corresponding author.

Abstract

The eastern Altun Shan is a crucial part of the Altun orogenic belt within the Tibetan Plateau. Study of the uplift rate and the related features in this area provides important clues for understanding the uplift mechanism of the Tibetan Plateau as a whole. As an important geomorphic element in landscape development, the fluvial system can record the relationship between tectonic activity and climatic change. In recent years, studies of the Channel Steepness Index K_{sn} , have been conducted by many researchers, using the geomorphological model of equilibrium channel longitudinal profiles, combining bedrock uplift and river incision and thus making it possible to extract rock uplift history from river profiles. This research show that regional rock uplift rate is a major factor in affecting the K_{sn} index. Regional tectonic activity and intensity, therefore, can be evaluated from variation in the K_{sn} index, which can provide a sensitive measure of uplift rate.

In this paper, the Digital Elevation Map 'ASTER GDEM', with a spatial resolution of 30 m, was utilized as basic data, and combined with ArcGIS and MATLAB software to extract the K_{sn} index from the equilibrium channel longitudinal profiles model. Meanwhile, we employed statistical methods to analyze the K_{sn} index.

Our results suggest that averaged K_{sn} indices, obtained from the subrange A, B, C, D, and E of the eastern Altun Shan (from west to east), are 70.93, 139.03, 108.85,

134.44 and 165.39, respectively. Further analysis implies that the variation in this index can be correlated with the distribution pattern of uplift rates within different regions. Its value increases gradually from west to east, reflecting regional uplift rate. Along the western section of the eastern Altun Shan, the uplift rate is slower and characterized by strike-slip movements, while its eastern part has uplifted faster and is controlled by thrust fault systems. Moreover, in contrast with the southern Altun Shan, the uplift rate of the northern part is high. These variations in uplift rate seem to be linked with “the imbricated thrusting transformation-limited extrusion model” of the Tibetan Plateau. Our results can be correlated with previous work on the active characteristics along the eastern Altyn Tagh Fault (ATF).

Key words: Eastern Altun Shan; Channel Steepness Index; uplift rate; fluvial incision

1. Introduction

The Altyn Tagh Fault (ATF) system, as the northern boundary of the Tibetan Plateau, is famous for its large amount slip (e.g., Molnar, 1975; Tapponnier et al., 1982; Xu et al., 1999; Yin et al., 2002; Xu et al., 2005; Cheng et al., 2016). Much research has been focused on its present geometric kinematics, dynamics and structural chronology (e.g., Wang, 1997; Ge et al., 2002; Yuan et al., 2006; Gold et al., 2011; Zhang et al., 2007). The large-scale strike-slip movement and Positive Flower Structure system led to elevation and exhumation of the middle and lower crust in the Altyn Tagh Range, finally forming the grand Altun Shan. During the Cenozoic period, the Altun Orogenic Belt has risen strongly with the uplift of the Tibetan Plateau. In recent decades, much work has focused upon the uplift of the Altun Shan (e.g., Jolivet et al., 1999; Wan et al., 2001; Jolivet et al., 2001; Chen et al., 2002; Ge et al., 2002; Yuan et al., 2006). These studies, however, only addressed the uplift history within certain specific periods, and with low resolution, because of the availability of chronological frameworks that were only approximate and difficult access to some field key sites (e.g., Zhu et al., 1990; Ge et al., 2004; Yuan et al., 2006). In contrast, the intensity and distribution pattern of tectonic uplift across the whole Altun Shan are less well known. Thus the aim here to outline the differentiation in tectonic activity and then further explore the growth mechanism of the Tibetan Plateau will constitute major challenges.

The eastern Altun Shan, which is intermediate between the Qilian Shan and Altun Shan, plays a key role in the understanding of structural evolution and in evaluation of differences in regional tectonic activities. In this paper, we extract fluvial channel-steepness indices and then analyze their distribution pattern along the eastern Altun Shan. For testing the accuracy of the channel steepness index as a digital geomorphic parameter to estimate the intensity of regional tectonic activity, these calculated indices were further correlated with measured fluvial incision rates in the region.

2. Regional Setting

The Indian and the Eurasian plates have converged and collided at an averaged velocity of 40–50 mm/a since 55 Ma, bringing about a series of orogenic movements and fault-belt growth in the Northern Tibetan Plateau (Molnar et al., 1987; Wittlinger et al., 1998; Tapponnier et al., 2001). The Altun orogenic belt, constraining the northern boundary of the Plateau, represents the frontier area of the Indian–Eurasian collision. Along this belt, a very large left-lateral slip fault system (termed ATF) forms the main boundary fault of the Northern Tibetan Plateau, separating two major inland basins, the Tarim and Qaidam Basins of north-western China. This fault reaches up to 1500~1600 km in length and plays an important role in controlling and accommodating the Cenozoic crustal deformation of the Plateau (Molnar et al., 1987; Ding, 1995; Deng et al., 2002; Yin et al., 2002; Xu et al., 2003; Xu et al., 2005; Cheng et al., 2016; Li et al., 2016).

<Fig. 1 is hereabout>

Our study mainly focuses upon the eastern Altun Shan (here referred as the Altun orogenic belt), where that mountain range converges with the Qilian Shan (Fig. 1). The Altun Shan has been uplifted as a NE–SW trending orogen, reaching up to 5753 m at its highest point, and with an N–S width of 25–35 km. Its northern front is steeper than its southern flank. A series of faults were formed along the eastern Altun Shan (Fig. 1A), together constituting the eastern ATF, which includes the northern ATF (F1), the Southern ATF (F2), the North Qaidam fault (F3), the Danghenanshan fault (F4), the Yemahe fault (F5), the North Danghenanshan fault (F6), a branch fault of the southern ATF (f2), and a branch fault of the Danghenanshan (f4). In detail, the eastern ATF, extending from Lapeiquan (W) to Subei (E) and with a length up to 200 km, plays a key role in accommodating the tectonic stress from the northern part of the Tibetan Plateau. Detailed research in this area has led to reporting of the active parameters of these faults (e.g., Ding, 1995; Deng et al., 2002; Xu et al., 2003; Li et al., 2016; Cheng et al., 2016). F1 is aligned in a WNW direction near the Lapeiquan, gradually turning to an ENE direction of 70–75°. At Qingyazi, it is characterized by a

left-lateral and right stepover, creating a multiple extrusion zone. The same tectonic geometric morphology also occurs along F2, which further extends eastward to connect with F4.

In Fig.1A, we can observe that the western section of F2, extending toward the west from Annanba, is shows a trend direction of ENE 70–75°, and then turning to the east near Annanba, is expressed as an ‘S’ type. F3, originating from the south flank of the Altun Shan, trends toward the SE as the boundary between the Qaidam basin and the Qilian Shan, and finally becomes hidden at Wulan (Ye et al., 1996; Pang et al., 2015). Since the Pliocene, this fault has evolved further, forming a series of right-lateral-slip-thrust-structures (Wang et al., 2005; Xiao et al., 2006).

Based on the digitized 1:50000 geological map (Fig.1B, Bureau of Geology and Mineral Resources of Gansu Province, 1989), the study area is dominated by the Paleoproterozoic quartz-mica schist, quartzite, amphibolite and granulite, and unconsolidated Quaternary deposits. Other lithologies, namely Middle and Neoproterozoic dolomitic marble, silica-banded carbonate, silty slate, Ordovician lava, Silurian volcano-clastic, Carboniferous mudstone, Oligocene sandstone, tonalite, quartz-diorite, granite, and various ultramafic rocks, are only distinguished sporadically in this area. In summary, the lithological distribution along the eastern Altun Shan is complex and diverse rather than a regular and uniform pattern (see Fig.1B).

3. Methodology: channel-steepness index

Recent decades have seen the application of geomorphic parameters, providing new insight into tectonic activity and regional uplift information in association with advances in tectonic geomorphology (e.g., Li et al., 1996; Pan et al., 2003, 2004, 2007; Hu et al., 2010; Zhang et al., 2010; Yang et al., 2013; Liang et al., 2015; Pan et al., 2015; Li et al., 2015). Research on shear-stress incision modelling has revealed that the detachment-limited rate of bedrock channel erosion (E) is a power function of upstream drainage area (A) and local channel slope (S) (Howard, 1994; Howard and

Kerby, 1983; Whipple and Tucker, 1999; Bridgland and Westaway, 2012):

$$E=K \cdot A^m \cdot S^n \quad (1)$$

Where (K) is the erosion coefficient, (m) is the area exponent, and (n) is the slope exponent, the value of which amalgamates many different variables that control erosional efficiency, including rock erodibility, sediment load, climate, erosion process, hydraulic geometry, and the return period for effective discharge episodes. At the same time, it is considered that at any point along a river profile, the change in height with time (dz/dt) is the difference between rock uplift (U) and erosion (E): (Howard, 1994; Snyder, et al., 2000; Kirby et al., 2003; Wobus et al., 2006; Ramsey et al., 2007; Hu et al., 2010; Burbank and Anderson, 2011; Kirby and Whipple, 2012; Pan et al., 2015).

$$dz/dt=U-E=U- K \cdot A^m \cdot S^n \quad (2)$$

For a steady-state profile in which channel elevation at a particular point does not change, dz/dt equals zero, and U equals E, and equation (2) can be solved for equilibrium slope (S_e) as follows:

$$S_e= (U/K)^{1/n} \cdot A^{-m/n} \quad (3)$$

In this context, the long profile of the river is a function of m/n , which is defined as the concavity and is typically designated as θ . The power-function relation implied by equation (3) has been observed empirically in many different geological settings (e.g., Hu et al., 2010; Pan et al., 2015; Li et al., 2016), with stream gradient described by:

$$S=K_s \cdot A^{-\theta} \quad (4)$$

The exponent K_s is channel-steepness index, which is similar in principle to the stream-gradient index developed by Hack (1973), but more generalized. The concavity index (θ) is generally found to be between 0.3 and 0.6 (Hack, 1957; Moglen and Bras, 1995). In any analysis of stream longitudinal profile, the relationships are implied by equations (5) and (6):

$$\theta = m/n \quad (5)$$

and

$$K_s= (U/K)^{1/n} \quad (6)$$

Where these conditions are met, the parameters $(U/K)^{1/n}$ and m/n can be estimated directly through regression of channel-gradient and drainage-area data. In order to compare the channel–steepness index under different drainage-area and concavity indices, researchers have used the reference concavity index (θ_{ref}) to calculate the normalized steepness index K_{sn} .

The variation in the channel normalized steepness index (K_{sn}) can still show a sensitive response to the difference in structural uplift activity, despite some limitations appearing within the reconstruction of regional uplift rate differences by the balanced river longitudinal profile model with a series of empirical tests (e.g., Hack, 1957; Moglen and Bros, 1995; Whipple and Tucker, 1999; Snyder et al., 2000; Kirby et al., 2003; Wobus et al., 2006; Hu et al., 2010; Burbank and Anderson, 2011; Kirby and Whipple, 2012; Wang et al., 2015; Li et al., 2016; Wang et al., 2016; Liu et al., 2016). This index is thus employed in this paper to analyze the distribution characteristics of regional tectonic activity and then further discuss the fault activity characteristics and differences along the eastern Altun Shan.

<Fig. 2 is hereabout>

Taking into account the significant differences in geomorphology and tectonic activity along the eastern Altun Shan, we have divided this studied area into five subranges, which are identified sequentially as A, B, C, D, and E, from west to east (see Fig. 2a for their extent). They are all cut through by F1 and F2. The peak within A reaches up to ~3923 m in comparison with the lowest altitude of ~2034 m, creating a local relief of ~1889 m. An intermontane basin in A, cut through by F2, was formed at the elevation of ~2810 m, close to the averaged elevation for A of 2809 m. F3 trends toward the northwest within B, intersecting with F2. The averaged elevation and local relief in B are ~4826 and ~2481 m, respectively. The extent of C is the largest of the subranges, and its averaged elevation and local relief reach the maximum values of ~3755 and 3580 m, and then decrease gently to ~3250 and ~2278 m in D (Fig. 4b). Due to the considerable relief, a series of deep gorges and the

highest peak of the Altun Shan occur within C, where f2 converging with F2 and F1 is apparently expressed by a W–E trending, arc-shaped fault system. The Altun Shan combines with the Qilian Shan within E, resulting in a complex fault system in which F4, f4, F5, and F6 are involved, as well as F1 and F2. The averaged elevation and local relief across E is ~3435 and 2594 m, respectively. Its landscape is characterized by a series of high mountains and a typical intermontane basin cut through by F2 and F4. In this paper, the ASTER GDEM, with a spatial resolution of 30 m in the vertical and 20 m in the horizontal, provides basic data covering the whole of the eastern Altun Shan. A combined method involving both ArcGIS and MATLAB was then employed to extract the channel-steepness index (K_{sn}) from the data, based on the equilibrium channel longitudinal profiles model (Whipple and Tucker, 1999; Snyder et al., 2000; Kirby et al., 2003; Wobus et al., 2006).

In detail, this K_{sn} index was extracted using the MATLAB script written by Snyder et al. (2000) and Kirby (2003), in which a referenced channel concavity index θ_{ref} was set as 0.45 and a 250 m window was adopted to smooth the obtained results. In addition, a contour sampling interval of 12 m was also set to calculate raw slope. The extracted K_{sn} indices from all drainage systems were then interpolated, finally presenting a distribution pattern over the eastern Altun Shan (Fig. 2b).

4. Results

In order to discuss the relationship between the activity behavior of these faults and the obtained K_{sn} indices along the eastern Altun Shan in detail, a total of 16 typical profiles, which are roughly perpendicular to the faults and across the regions with significant variation in value, have been reconstructed within the five subranges (Fig. 2b). These obtained profiles are shown in Fig. 3, based on which the average K_{sn} index value has been calculated for each profile.

<Fig. 3 is hereabout>

Overall, those K_{sn} indices extracted from the northern front are rather high compared with those from the southern flank, except the profiles ② and ④. This distribution pattern is in agreement with the topographic characteristics of the eastern Altun Shan (which has a steeper northern front than southern flank). Profiles ② and ④, however, cross precisely through regions where the stress of F1 and F2 has been adjusted, probably leading to their mismatch. Owing to intense strike-slip activity by F1 and F2, their interior regions are dominated mainly by horizontal movement, marked by the lower K_{sn} indices along these profiles. In Profiles ⑮ and ⑯, the K_{sn} indices show a marked increase in the confluence area between the eastern Altun Shan and western Qilian Shan; strike-slip movement is perhaps resisted by the western Qilian Shan, resulting in a region in which tectonic stress has been concentrated. This abrupt increase in K_{sn} indices in profiles ⑮ and ⑯ may be linked with this high stress.

<Fig. 4 is hereabout>

Based on the distribution pattern of K_{sn} indices along the eastern Altun Shan (Fig. 2b), the average K_{sn} index for each subrange has been calculated (Fig. 4a). An approximate trend of change has been outlined, in which these average K_{sn} indices show a general and gradual increase between subranges A to E (from west to east), except C, where the main peak of the Altun Shan occurs. Based on the same DEM data, a 240-km-long and 40-km-wide swath window across the five subranges was selected for the topographic analysis of maximum, minimum, mean, and local relief (Fig. 4b). Their variation seems to be correlated with the distribution pattern of K_{sn} indices, implying that strike-slip displacement by the eastern Altun Shan is gradually cumulative eastwards (Xu et al., 2005).

5. Discussion

5.1. Analysis of factors influencing the K_{sn} index

On the basis of the shear-stress incision model (Snyder et al., 2000), the K_{sn} index can show a sensitive response to variations in bedrock lithology, precipitation, sedimentary load, and rock uplift rate (e.g., Hack, 1957; Moglen and Bros, 1995; Whipple and Tucker, 1999; Snyder et al., 2000; Kirby et al., 2003; Wobus et al., 2006; Hu et al., 2010; Burbank and Anderson, 2011; Kirby and Whipple, 2012; Pan et al., 2015; Wang et al., 2015; Li et al., 2016; Wang et al., 2016; Liu et al., 2016). The geology of the eastern Altun Shan is dominated by regional metamorphic rocks, including the Proterozoic quartz schist, quartzite, and amphibolite. In contrast, granite, gabbro, and ultrabasic/mafic rocks can be identified only sporadically, within a very limited area (Fig.1B). Over the extent of the eastern Altun Shan, therefore, there is a roughly uniform lithological distribution presents pattern, which seems unlikely to be responsible for the remarkable change in the K_{sn} index.

The eastern Altun Shan is located within a typical desert environment, with a mean annual precipitation that reaches only 110.0 mm, and is characterized by a rather high mean annual evaporation, at 2495.2 mm (Resource and Environment Data Cloud Platform of China: <http://www.resdc.cn/>). All the rivers originating from the eastern Altun and debouching northward into the desert are therefore ephemeral. The mean annual precipitation within the mountains is a little higher than in their frontal zones, reaching 200.0–250.0 mm. Moreover, from west to east, along the eastern Altun Shan, mean annual precipitation is see to increase slowly from 27.0 to 183.0 mm, with average annual evaporation also increasing from 1630.0 to 2500.0 mm. According to Hu et al. (2010), however, the K_{sn} index has an inverse correlation with mean annual precipitation within arid and semi-arid regions, so the variation in the K_{sn} index along the eastern Altun Shan cannot be attributed to the increasing mean annual precipitation.

<Fig. 5 is hereabout>

In general, the variation in K_{sn} index can also be linked with sedimentary load (Snyder et al., 2000; Kirby et al., 2003; Wobus et al., 2006; Hu et al., 2010; Burbank and Anderson, 2011; Kirby and Whipple, 2012; Pan et al., 2015). Based on field investigation, the river channel types in the eastern Altun Shan mainly comprise exposed bedrock riverbeds, alluvial rivers, and accumulation channels, as well as combinations of these (Fig.5). In addition, these are all ephemeral rivers, which, in combination with the notably low mean annual precipitation, results in limited sedimentary loads. Along the eastern Altun Shan, sedimentary loads are indeed probably approximately equal, in contrast to the striking variation in the K_{sn} index.

5.2. Correlation between K_{sn} index and fluvial incision rate

Considering the rather limited impact of lithology, precipitation, and sedimentary load on the K_{sn} index along the eastern Altun Shan, rock uplift rate is employed here to link with the variation of this index. Previous work by Hu et al. (2010) and Pan et al. (2015) has suggested that the change in K_{sn} index within the Qilian Shan can probably be attributed to variation in rock uplift rate. Further analysis has revealed that there is a positive correlation (e.g., Hack, 1957; Moglen and Bros, 1995; Whipple and Tucker, 1999; Snyder et al., 2000; Kirby et al., 2003; Wobus et al., 2006; Hu et al., 2010; Burbank and Anderson, 2011; Kirby and Whipple, 2012; Wang et al., 2015; Li et al., 2016; Wang et al., 2016; Liu et al., 2016).

Controlled by a series of strike-slip thrust faults, the eastern Altun Shan has been strongly uplifted during the Cenozoic (Yin et al., 2002; Xu et al., 2005; Cheng et al., 2016). These faults remain active at the present day, so that this mountain range maintains a tectonically uplifting setting (Cheng et al., 2016)(Fig.1). In general it is thought that tectonic or rock uplift rate can be evaluated from fluvial incision rate (Bridgland et al., 2000, 2007, 2012; Pan et al., 2003, 2007, 2012; Vandenberghe, 2008; Westaway et al., 2009a). At the eastern end of the eastern Altun Shan, the Daobo, Xiaoobo, and Changcaogou rivers flow northward through the strike-slip

thrust faults, debouching into the desert (Fig. 1A). A series of terrace sequences has been formed along these rivers (e.g. Chen et al., 2012). In order to investigate the pattern of the incision by these rivers, from west to east, a total of 5 Optically Stimulated Luminescence (OSL) samples was taken from sand lenses within the gravels accumulated on terraces T1 and T2 (Fig.6).

In sampling, a 25-cm-long stainless steel tube was hammered horizontally into the sediments in freshly cleaned vertical sections. Then, immediately after removal, the tube was sealed with tinfoil and plastic tape at both ends. In the OSL Chronology Laboratory in the Key Laboratory of Western China's Environmental Systems (Ministry of Education), Lanzhou University, 90–125 μm quartz grains were selected and purified following the procedure of Zhao and Li (2002) and Fan et al. (2010). Luminescence signals were measured for 2-mm-diameter small aliquots using an automated Risø TL/OSL-DA-20 reader.

The OSL signal was measured using the modified single-aliquot regenerative protocol (Banerjee et al., 2001) to eliminate the potential contribution of any infrared stimulated luminescence (IRSL) signals from feldspar inclusions within the quartz crystals, and the post-infrared (IR) OSL signal was used to obtain the D_e values of the quartz fractions. The detailed protocol was described by Fan et al. (2016). The environmental dose rate was calculated from the concentrations of U, Th, and K in the samples and from the contribution of cosmic rays. The water content was estimated according to the natural water content and saturated water content. Age calculation uses the central age model and represents a 2σ uncertainty.

On the basis of the dating results from these samples (Table 1), with reference to related terrace heights, the average rates of incision by the Daebo, Xiaoebo, and Changcaogou rivers were calculated and are shown in Table 2. A significant trend can be clearly observed, in which the rate of incision increases progressively from west to east, in good agreement with other researchers (e.g. Xu et al., 2003; Chen et al., 2012). Owing to the resistance of the Qilian Shan, the deformation of these strike-slip thrust faults has been transformed into vertical thrust style at the eastern end of the eastern Altun Shan (Chen et al., 2002; Deng et al., 2002; Xu et al., 2003,

2005; Zheng et al., 2013; Cheng et al., 2016). The pattern of fluvial incision may thus indicate an eastward increasing trend in tectonic uplift rate (Ge et al., 2004; Xu et al., 2005; Li et al., 2015). Along the eastern Altun Shan, the variation in the K_{sn} index is in good agreement with the increase in uplift rate from west to east, confirming its tectonic implication (Deng et al., 2002; Xu et al., 2003, 2005). GPS observation by Zhang et al. (2004, 2007) and Li et al. (2015) also suggests that the left-lateral slip rate on fault F1 declines from west to east, in response to this transformation of tectonic style at the eastern end of the eastern Altun Shan.

<Table 1 is hereabout>

<Table 2 is hereabout>

<Fig. 6 is hereabout>

5.3. Uplift and lateral growth of the Tibetan Plateau revealed by the variation in K_{sn} index

The eastern ATF, as the northern boundary of the Tibetan Plateau, accommodates the force from the Indian plate, by the way of left-lateral strike slip motion (Molnar et al., 1975; Molnar et al., 1987; Ding, 1995; Cui, 1999; Deng et al., 2002; Yin et al., 2002; Westaway, 2009b; Xu et al., 2003). During the late Pleistocene, the maximum slip rate at the west end of this fault system has reached up to 30 ± 20 mm/a (Xu et al., 2003). According to the K_{sn} index distribution pattern, however, this rate decreases progressively eastward. At the east end of the eastern ATF, a remarkably reduced rate of 11.0 mm/a has been estimated (Xu et al., 2003). In the growth model for the Tibetan Plateau of Tapponnier et al. (1982, 2001), the great crustal shortening between the Indian and Eurasian plates is mainly absorbed by a series of strike-slip fault systems, bringing about rapid escape of the extruded mass. Based on further analysis of the geodetic data, in combination with chronological study, the eastward escape or extrusion of the Tibetan Plateau is nevertheless

regarded as limited (Deng et al., 2002; Xu et al., 2003, 2005). Along the eastern ATF, some active thrust faults with a NW trend splay from this fault and propagate southeastward, creating two sets of triple junctions (Fig. 1A). Slip vector analyses argue that the sinistral slip rates from west to east across these junctions have decreased significantly since Pleistocene (Xu et al., 2003). Their loss has been considered to be transformed into local crustal shortening perpendicular to the active thrust faults, associated with strong uplift of the Qilian Shan (Ding, 1995; Cui et al., 1999; Xu et al., 2003). As a result, the distribution pattern of K_{sn} index along the eastern Altun Shan, obtained in this study, is in good agreement with “the imbricated thrusting transformation-limited extrusion model” of the Tibetan Plateau (Deng et al., 2002; Xu et al., 2003, 2005).

6. Conclusions

In this study, the K_{sn} index over the eastern Altun Shan has been extracted from the ASTER GDEM and used as basic data for analysis. Its distribution pattern has been clearly observed to represent a general increase in value from west to east along this mountain range. Further relative analysis has revealed that the variation in this index probably results from changes in uplift rate, rather than in lithology, precipitation, or sedimentary load. In fact, our chronological study, combined with terrace archives, has confirmed that the incision rate increases gradually eastward, reflecting an eastward rise in uplift rate. Thus the K_{sn} index distribution pattern within the eastern Altun Shan provides notable support for the argument for “the imbricated thrusting transformation-limited extrusion model” of the Tibetan Plateau.

Acknowledgments

We are grateful to Haifeng Zhang, Pengju Fan, Shibo Tuo, and Bing Guo for assistance with the field work. The comments by the two anonymous referees, and the special issue editor, Xianyan Wang, have led to considerable improvements and are

gratefully acknowledged. This study is financially supported by the National Natural Science Foundation of China (Grant no. 41730637, 41871001, and 41571003) and the land resource survey project by Geological Survey of China (Grant no. DD20160012).

References

Bridgland D R, and Westaway R. The use of fluvial archives in reconstructing landscape evolution: the value of sedimentary and morphostratigraphical evidence [J]. *Netherlands Journal of Geosciences*, 2012, 91(1-2): 5-24, doi: org/10.1017/S0016774600000536

Bridgland D R, Demir T, Seyrek A, Pringle M, et al. Dating Quaternary volcanism and incision by the River Tigris at Diyarbakir, SE Turkey[J]. *Journal of Quaternary Science*, 2007, 22: 387-393.

Bridgland D R. River terrace systems in north-west Europe: an archive of environmental change, uplift and early human occupation[J]. *Quaternary Science Reviews*, 2000, 19: 1293-1303.

Banerjee, D., Murray, A., Bøtter-Jensen, L., and Lang, A., Equivalent dose estimation using a single aliquot of polymineral fine grains: *Radiation Measurements*, 2001, v. 33, no. 1, p. 73-94.

Burbank D W, Anderson R S. *Tectonic Geomorphology*. Massachusetts: Blackwell Science, 2011, 247~251.

Bureau of Geology and Mineral Resources of Gansu Province. *Regional Geology of Gansu Province*, 1989.

Chen Xuanhua, Yin An, Gao Jian et al. Preliminary study on regional thermal history in the Altyn region. *Geological Review*, 2002, 48(Suppl.): 146~152.

Chen Yiwei, Li Shenghua, Li Bo. Slip rate of the aksay segment of Altyn Tagh Fault

- revealed by OSL dating of river terraces. *Quaternary Geochronology*, 2012, (10): 291-299. doi: 10.1016/j.quageo.2012.04.012
- Cheng Feng, Jolivet Marc, Fu Suotang et al. Large-scale displacement along the AltynTagh Fault (North Tibet) since its Eocene. *Tectonophysics*, 2016, (677/678): 261~279
- Cui Junwen, Tang Zhemin, Deng Jinfu et al. *Altyn Fault System*. Beijing: Geological Publishing House, 1999. 1~249
- Deng Qidong, Zhang Peizhen, Ran Yongkang et al. Basic characteristics of active tectonics of China. *Science in China (Series D)*, 2002, 32(12):1020~1030
- Ding Guoyu. Paleoearthquakes along the Altyn Active Fault and its segmentation. *Quaternary Sciences*, 1995, 15(2): 97~106
- Fan, Y., Zhao, H., and Chen, F., The equivalent dose of different grain size quartz fractions from lakeshore sediments in the arid region of north China: *Quaternary Geochronology*, 2010, v. 5, no. 2, p. 205–211. Fan, Y., Zhang, F., Zhang, F., Liu, W., Chen, X., Fan, T., Wang, Y., Chen, F., and Lai, Z., History and mechanisms for the expansion of the Badain Jaran Desert, northern China, since 20 ka: Geological and luminescence chronological evidence: *The Holocene*, 2016, v. 26, no. 4, p. 532–548.
- Ge Xiaohong, Liu Yongjiang, Ren Shoumai et al. Uplift dynamics of the Qinghai-Tibet Plateau and Altyn fault. *Geology in China*, 2002, 29(4): 346~350
- Ge Xiaohong, Ren Shoumai, Liu Yongjiang et al. Last rapid uplift of Qinghai-Tibet Plateau and the Australasian event of meteorites. *Quaternary Sciences*, 2004, 24(1): 67~73
- Gold R D, Cowgill E, Arrow Smith J R et al. Faulted terrace risers place new constraints on the Late Quaternary slip rate for the central Altyn Tagh fault, northwest Tibet. *GSA Bulletin*, 2011,123(5/6): 958~978
- Hack J T. Stream-profile analysis and stream-gradient index[J]. *Journal of Research of*

- the US Geological Survey, 1973, 1 (4): 421-429.
- Hack J T. Studies of longitudinal stream profiles in Virginia and Maryland. Geological Survey Professional Paper, 1957, 294 (B) : 42~97
- Howard A D, Kerby G Channel changes in Badlands. Geological Society of America Bulletin, 1983, 94 (6) : 739~752
- Howard A D. A detachment-limited model of drainage basin evolution. Water Resources Research, 1994, 30(7): 2261~2285
- Hu Xiaofei, Pan Baotian, Kirby E et al. Spatial differences in rock uplift rates inferred from channel steepness indices along the northern flank of the Qilian Mountain, northeast Tibetan Plateau. Chinese Science Bulletin , 2010 , 55(27~28): 3205~3214.
- Jolivet M, Brunel M, Seward D, et al. Mesozoic and Cenozoic tectonics of the northern edge of the Qinghai- Tibet Plateau Qinghai-Tibet Plateau: fission-track constraints. Tectonophysics, 2001, 343(1/2): 111~134
- Jolivet M, Roger F, Arnaud, N, et al. Exhumation history of the Altynshan with evidence for the timing of the subduction of the Tarim block beneath the Atlyn Tagh system, North Tibet. Earth & Planetary Sciences, 1999, 329: 749~755
- Kirby E, Whipple K X, Tang W Q et al. Distribution of active rock uplift along the eastern margin of the Tibetan Plateau: Inferences from bedrock channel longitudinal profiles. Journal of Geophysical Research: Solid Earth, 2003, 108 (B4) :2217
- Kirby E, Whipple K X. Expression of active tectonics in erosional landscapes. Journal of Structural Geology, 2012, 44: 54~75
- Li Jijun, Fang Xiaomin, Ma Haizhou et al. Late Cenozoic geomorphic evolution of the upper reaches of the Yellow River and the Tibetan Plateau uplift. Science in China (Series D), 1996, 26(4): 316~322

- Li Kang, Xu Xiwei, Luo Hao et al. Paleoseismic events in BanGuoBa trench along AKSay segment of the AltynTagh Fault zone. *Seismology and Geology*, 2016, 38(3): 670~679
- Li Qiong, Pan Baotian, Gao Hongshan et al. Bedrock channel width responses to differential tectonic uplift in eastern Qilian Mountain. *Quaternary Sciences*, 2015, 35(2):453-464.
- Li Xiaoqiang, Wang Jun, XiongRenwei et al. The response of the channel steepness index to the difference of uplift rate in the Liupanshan mountain area. *Quaternary Sciences*, 2016, 36 (2):443~452
- Li Yuhang, Wang Qingliang, Cui Duxin et al. Inversion of present-day fault slip rate along Altyn Tagh Fault constrained by GPS Data. *Seismology and Geology*, 2015, 37(3): 869~879
- Liang Hongying, Lin Zhou. Characterization of landform evolution stages of the Ailao Shan Mountain range. *Quaternary Sciences*, 2015, 35 (1):38~47.
- Liu Xingwang, Yuan Daoyang, Wu Zhao et al. Differential activities along the Liupanshan Mountain fault zone and its influence on uplift of the Liupanshan Mountain. *Quaternary Sciences*, 2016, 36(4): 898~906
- Merritts D, Bull W B. Interpreting quaternary uplift rates at the Mendocino triple junction, northern California, from uplifted Marine terraces. *Geology*, 1989, 17 (11) : 1020~1024
- Moglen G E, Bras R L. The effect of spatial heterogeneities on geomorphic expression in a model of basin evolution. *Water Resource Research*, 1995, 31 (10) 2613~2623
- Molnar P, Burchfiel B C, Liang K et al. Geomorphic evidence for active faulting in the Altyn Tagh and northern Tibet and qualitative estimates of its contribution to the convergence of India and Eurasia. *Geology*, 1987, 15 (3) :249~253

- Molnar P, Tapponnier P. Cenozoic tectonic of Asia: Effect of a continental collision. *Science*, 1975, 189: 419~426
- Pan B. T., Gao H. S., Yuan B. Y., and Li J. J. Step-like landforms and uplift of the Qinghai-Xizang Plateau [in Chinese with English abstract]. *Quat. Sci.*, 2004, 24(1), 50–57.
- Pan Baotian, D. Burbank, Wang Y. X., Wu G J., Li J. J., and Guan Q. Y. A 900 ky record of strath terrace formation during glacial-interglacial transitions in northwest China. *Geology*, 2003, 31(11), 957–960, doi:10.1130/G19685.1.
- Pan Baotian, Li Qiong, et al. Bedrock channels response to differential rock uplift in eastern Qilian Mountain along the northeastern margin of the Tibetan Plateau. *Journal of Asia Earth Sciences*, 2015. 15, 100: 1-19.
- Pan, B. T., Gao H. S., Wu G J., Li J. J., Li B. Y., and Ye Y. G. Dating of erosion surface and terraces in the eastern Qilian Shan, northwest China, *Earth Surf. Proc. Landforms*, 2007, 32(1), 143–154, doi:10.1002/esp.1390.
- Pan, B. T., Hu X. F., Gao H. S., Hu Z. B., Cao B., Geng H. P., and Li Q. Y. Late Quaternary river incision rates and rock uplift pattern of the eastern Qilian Shan Mountain, China. *Geomorphology*, 2013, 184, 84–97, doi:10.1016/j.geomorph.2012.11.020.
- Pang Wei, He Wengui, Yuan Daoyang et al. Paleoseismic characteristics of Dachaidan Fault in Qinghai. *Journal of Earth Sciences and Environment*, 2015, 37(3): 87~103
- Ramsey LA, Walker R T, Jackson J. Geomorphic constraints on the active tectonics of southern Taiwan. *Geophysical Journal International*, 2007, 170(3): 1357~1372
- Snyder N P, Whipple K X, Tucker G E et al. Landscape response to tectonic forcing: digital elevation model analysis of stream profiles in the Mendocino triple junction region, northern California. *Geological Society of America Bulletin*, 2000, 112 (8) : 1250~1263

- Tapponnier P, Peltzer G, Le Dain A Y. Propagating extrusion tectonics in Asia: New insights from simple experiments with plasticine. *Geology*, 1982, 10 (12) :611~617
- Tapponnier P, Zhi Q X, Roger F et al. Oblique stepwise rise and growth of the Tibet Plateau. *Science*, 2001, 294 (5547) :1671~1677
- Vandenberghe J. The fluvial cycle at cold-warm-cold transitions in low-land regions: a refinement of theory[J]. *Geomorphology*, 2008, 98: 275-284.
- Wan Jinglin, Wang Yu, Li Qi et al. FT evidence of northern Altyn uplift in Late Cenozoic. *Bulletin of Mineralogy, Petrology and Geochemistry*, 2001, 20(4): 222~224
- Wang Buqing, Xiao Ancheng, Cheng Xiaogan et al. Geometry and kinematics of Cenozoic right-lateral strike-slip thrust structural belt in the north margin of the Qaidam Basin. *Journal of Zhe Jiang University (Science Edition)*, 2005, 35(2): 225~230
- Wang Erchie. Displacement and timing along the northern strand of the Altyn Tagh fault zone, northern Tibet. *Earth and Planetary Science Letters*, 1997,150(1/2): 55~64
- Wang Nairui, Han Zhiyong, Li Xusheng et al. Tectonic uplift of Mt. Lushan indicated by the steepness indices of the river longitudinal profiles. *Acta Geographica Sinica*, 2015, 70(9): 1516~1525.
- Wang Yizhou, Zhang Huiping, Zheng Dewen et al. Stream power incision model and its implications: Discussion on the urgency of studying bedrock channel across the Tibetan Plateau. *Quaternary Sciences*, 2016, 36(4): 884~897.
- Wang Yizhou, Zhang Huipin, Zheng Dewen et al. How a stationary knickpoint is sustained: new insights into the formation of the deep Yarlung Tsangpo Gorge. *Geomorphology*, 2017a, 285, 28–43.

- Wang Yizhou, Zhang Huiping, Zheng Dewen, et al. Coupling slope–area analysis, integral approach and statistic tests to steady-state bedrock riverprofile analysis. *Earth Surf. Dyn.*, 2017b.5: 145–160.
- Wang Yizhou, Zheng Dewen, Pang jianzhang, et al. Using slope-area and apatite fission track analysis to decipher the rock uplift pattern of the Yumu Shan: new insights into the growth of the NE Tibetan Plateau. *Geomorphology*, 2018, 308: 118–128.
- Wang Yizhou, Zheng Dewen, Zhang Huiping et al. The distribution of active rock uplift in the interior of the western Qilian Shan, NE Tibetan: Inference from bedrock channel profiles. *Tectonophysics*, 2019, 759: 15~29.
- Westaway R, Bridgland D R, Sinha R & Demir T. Fluvial sequences as evidence for landscape and climatic evolution in the Late Cenozoic: A synthesis of data from IGCP 518[J]. *Global and Planetary Change*, 2009a, 68: 237-253 (Editorial for special issue by the same name).
- Westaway R, Guillou H, Seyrek A, Demir T, Bridgland D R, Scaillet S & Beck A. Late Cenozoic surface uplift, basaltic volcanism, and incision by the River Tigris around Diyarbakir, SE Turkey[J]. *International Journal of Earth Sciences*, 2009b, 98: 601-625.
- Westaway R. Active crustal deformation beyond the SE margin of the Tibetan Plateau: constraints from the evolution of fluvial systems[J]. *Global and Planetary Change*, 2009, 69: 395-417.
- Whipple K X, Tucker G E. Dynamics of the stream-power river incision model: Implications for height limits of mountain ranges, landscape response timescales, and research needs. *Journal of Geophysical Research*, 1999, 104 (B8) : 17661~17674.
- Wittlinger G, Tapponnier P, Poupinet G. Tomographic evidence for localized lithospheric shear along the Altyn Tagh Fault. *Science*, 1998, 282 (5386) :74~76.

- Wobus C, Whipple K X, Kirby E et al. Tectonics from topography: procedure, promise, and pitfalls. *Geological Society of America Special Paper*, 2006, 398 (12) :55~74.
- Xiao Ancheng, Yang Shufeng, Chen Xiaogan et al. Right-lateral strike-slip thrust system and its dynamics along the northern margin of Qaidam Basin. *Oil & Gas Geology*, 2006, 27(4): 482~494.
- Xu Xiwei, Tapponnier P, Van Der Woerd J et al. Late Quaternary sinistral slip rate along the Altyn Tagh fault and its structural transformation model. *Science in China, Ser D*, 2005, 48(3):384~397.
- Xu Xiwei, Wen Xueze, Zheng Rongzhang et al. Pattern of latest tectonic motion and its dynamics for active blocks in Sichuan-Yunnan region, China. *Science in China, Ser D*, 2003, 46(2):210-226.
- Xu Zhiqin, Yang Jingsui, Zhang Jianxin et al. A comparison between the tectonic units on the two sides of the Altyn sinistral strike-slip fault and the mechanism of lithospheric shearing. *Acta Geologica Sinica*, 1999, 73(3): 193~205.
- Yang Xiaoping, Li An, Huang Weiliang. Tianshan Mountains Activities fold belt during the Late Quaternary uplift difference. *Science China: Earth Sciences*, 2013, 56(5): 794~805.
- Ye Jianqing, Sheng Jun, Wang Yipeng et al. Tectonic Activity along the Northern Margin of Qindam Basin. Beijing: Seismological Press, 1996. 170~180.
- Yin An, Rumelhart P E, Butler R, et al. Tectonic history of the Altyn Tagh fault system in northern Tibet inferred from Cenozoic sedimentation. *GSA Bulletin*, 2002, 114(10): 1257-1295.
- Yuan Sihua, Liu Yongjiang, Ge Xiaohong et al. Advance in study of Mesozoic-Cenozoic uplift history of the Altyn Mountains. *Global Geology*, 2006, 25(2):164~171 .

- Zhang Huiping, Zhang Peizhen, Yuan Daoyang et al. Differential landscape development of the central N-S seismic zone and its relation to the west Qingling tectonic belt. *Quaternary Sciences*, 2010, 30 (4):803~811.
- Zhang P Z, Molnar P, Xu X W. Late Quaternary and present-day rates of slip along the Altyn Tagh fault, northern margin of the Tibetan Plateau. *Tectonics*, 2007, 26: TC5010, doi: 10.1029/2006TC002014.
- Zhang, P. Z., Shen Z. K., Min W., Gan W. J., and Burgmann R. Continuous deformation of the Tibetan Plateau from global positioning system data. *Geology*, 2004, 32(9), 809–812, doi:10.1130/G20554.1.
- Zhao, H., and Li, S., *Luminescence Isochron Dating: A New Approach with Different Grain Sizes*: Oxford, Radiation Protection Dosimetry, 2002, v. 101, no. 1–4, p. 333–338, doi: 10.1093/oxfordjournals.rpd.a005996. Zheng, W. J., Zhang H. P., Zhang P. Z., Molnar P., Liu X. W., and Yuan D. Y. Late Quaternary slip rates of the thrust faults in western Hexi Corridor (Northern Qilian Shan, China) and their implications for northeastward growth of the Tibetan Plateau. *Geosphere*, 2013, 9(2), 342–354, doi:10.1130/GES00775.1.
- Zhu Yunzhu, Zhong Jianhua, Wu Bihao et al. Preliminary approach to relationship between uplifting history of Altyn mountains and salt-forming condition in Tarim. *Oil & Gas Geology*, 1990, 11(2): 136~143.

Table Captions

Table 1. OSL sample information and analysis data.

Table 2. Terrace data and river incision rates.

Figure Captions

Fig. 1. Topographic and geological map of the eastern Altun Shan. (A) Major fault systems, rivers, and mountains across the eastern Altun Shan. The inset map displays the location within the Tibetan Plateau. Numerous ephemeral rivers develop along the northern and southern front of the eastern Altun Shan, and cutting through these fault systems. According to Xu et al. (2005), some active faults with NW trend splay from faults F1 and F2 and propagate southeastward, creating two sets of triple junctions, their extent constrained by the dotted circle. The rivers with OSL sampling positions are marked by red pentagon, in which the insert numbers 1, 2, and 3 represent the Daebo, Xiaoabo, and Changcaogou rivers, respectively. (B) Lithological information from the Chinese geological map, with a scale of 1:200,000 (Bureau of Geology and Mineral Resources of Gansu Province, 1989.). In the eastern Altun Shan, the dominant lithologies are regional metamorphic rocks, presenting a generally uniform pattern.

Fig. 2. Distribution map of the extracted K_{sn} , along the eastern Altun Shan. (a) The topographic map was divided into 5 subranges, named as A, B, C, D, and E, from west to east along the eastern Altun Shan. (b) The K_{sn} indices obtained from the above 5 subranges have been superimposed onto the topographic map of the eastern Altun Shan. In order to analyze their distribution pattern further, some 16 profiles were established within these subranges. They were numbered consecutively from ① to ⑯, corresponding with the profile numbers in Fig. 3.

Fig. 3. K_{sn} index profiles. In each profile, the vertical and horizontal axes depict K_{sn} index and distance, respectively. Their positions are indicated in Fig. 2. For each

profile, an average K_{sn} index has been calculated, and is denoted by dotted lines. In general, the K_{sn} indices extracted from the northern front of the eastern Altun Shan are higher than those from the southern flank, except for profiles ② and ④. The characteristics of these faults that were cut through by the profiles are shown on the K_{sn} index variation curves.

Fig. 4. K_{sn} index distribution pattern combined with topographic characteristics over the extent of the eastern Altun Shan. (a) K_{sn} index distribution pattern. The numbers along the horizontal axis express the same profiles as in Fig. 3. Their average K_{sn} indices are indicated by black dots, which were further connected with each other to point out an eastward increasing tendency. The green bars are the average K_{sn} indices over the five subranges along the eastern Altun Shan. See Fig. 2 for their detailed extent. (b) Maximum, minimum, mean, and local relief topography along a 240-km-long and 40-km-wide swath window across the same extent of the eastern Altun Shan. On this swath plot, the extent of major topographic features over the five subranges is displayed. Their variation seems to be correlated with the distribution pattern of K_{sn} indices.

Fig. 5. River channel types in the eastern Altun Shan. (A) Alluvial riverbed with thin gravel layer. (B) Example of bedrock riverbed. Numerous typical knickpoints have been observed in our field investigation, occurring along the rivers in the eastern Altun Shan, two of which are presented in A and B. (C) A complex riverbed pattern, including exposed bedrock riverbed, alluvial river, and accumulation channel. (D) Accumulation channel with thick gravel layer.

Fig. 6. Fluvial terraces formed by the Daebo, Xiaoebao, and Changcaogou Rivers at the east end of the eastern Altun Shan. (A) Terrace T1 of the Daebo. Its height above the riverbed is indicated, as is the age of an OSL sample taken from its gravel in order to calculate incision rate. (B) Age and height of Daebo terrace T2. (C) Terraces T1 and T2 of the Xiaoebao. Terrace T2 has been deformed by northward thrust faults. Its age and height were obtained to determine the incision rate. (D) Details of the yellow

dashed box within C to display the conglomerate wedge accumulated in the thrust nappe. (E) Terrace sequence of the Changcaogou. The age and height of terrace T3 are indicated. (F) Age and height of terrace T2 of the Changcaogou, with underlying deformed bedrock.

ACCEPTED MANUSCRIPT

Table 1: OSL sample information and analysis data.

Sample ID	Location /Terrace	Material	Latitude (°N)	Longitude (°E)	Altitude (m)	Burial depth (m)	Water content (%)	Equivalent dose(Gy)	Dose rate (Gy/ka)	OSL Age (ka)
DEB01	Daebo /T1	Fluvialsand	39.3792	94.1100	2758	2.0	10±5	55.5±1.5	3.71±0.26	14.9±1.1
DEB02	Daebo /T2	Fluvialsand	39.3790	94.1074	2807	6.5	10±5	114.0±1.8	3.57±0.25	31.9±2.3
XEB02	Xiaoeb0/T2	Fluvialsand	39.3973	94.1982	2628	4.5	10±5	56.3±6.1	3.46±0.24	16.3±2.1
CCG01	Changcaogou/ T2	Fluvialsand	39.4144	94.3005	2677	4.2	10±5	98.7±6.9	3.90±0.28	25.3±2.5
CCG02	Changcaogou/T3	Fluvialsand	39.4144	94.3005	2753	1.5	10±5	329.0±14.5	3.09±0.21	106.4±8.7

Table 2: Terrace data and river incision rates.

River channel	Terrace order	Age (ka)	Terrace height (m)	Incision rate(mm/a)
Daebo	T2	31.9±2.3	18.4	0.58±0.05
	T1	14.9±1.1	7.5	0.50±0.03
Xiaoebo	T2	16.3±2.1	12.0	0.73±0.07
Changcaogou	T3	106.4±8.7	111.0	1.04±0.08
	T2	25.3±2.5	23.0	0.90±0.07

Highlights

- Along the eastern Altun Shan, the obtained index K_{sn} shows a rough tendency of increasing eastward.
- The index K_{sn} from the north front of the eastern Altun Shan is higher than that from the south flank.
- This distribution pattern of the index K_{sn} is translated into the different uplift along the eastern Altun Shan.
- The difference in uplift rate can be evaluated well by the fluvial incision rate obtained by terrace archives.
- The analysis of the index K_{sn} along the eastern Altun Shan provides an excellent insight into the argument for extrusion model of the Tibetan Plateau.